scientific reports

Check for updates

OPEN

Dissecting resilience curve archetypes and properties in human systems facing weather hazards

Chia-Wei Hsu✉ & Ali Mostafavi

Resilience curves have been widely used for conceptualizing and representing specific aspects of resilience behavior during hazard events; however, their use has often remained conceptual with limited data-driven characterization and empirical grounding. While broader community resilience encompasses multiple social, economic, and infrastructure dimensions, targeted analyses of specific systems can provide valuable insights into resilience patterns. Empirical characterizations of resilience curves provide essential insights regarding the manner in which differently impacted systems of communities absorb perturbations and recover from disruptions. To address this gap, this study examines human mobility resilience patterns following multiple weather-related hazard events in the United States by analyzing more than 2000 empirical resilience curves constructed from high-resolution location-based mobility data. These empirical resilience curves are then classified into archetypes using k-means clustering based on various features (e.g., residual performance, disruption duration, and recovery duration). Three main archetypes of human mobility resilience are identified: Type I, with rapid recovery after mild impact; Type II, exhibiting bimodal recovery after moderate impact; and Type III, showing slower recovery after severe impact. The results also reveal critical thresholds, such as the bimodal recovery breakpoint at a 20% impact extent (i.e., function loss), at which the recovery rate decreases, and the critical functional threshold at a 60% impact extent, above which recovery rate would be rather slow. The results show that a critical functional recovery rate of 2.5% per day is necessary to follow the bimodal resilience archetype when impact extent exceeds 20%. These findings provide novel and important insights into different resilience curve archetypes and their fundamental properties. Departing from using resilience curves as a mere concept and visual tool, the data-driven specification of resilience curve archetypes and their properties improve our understanding of the resilience patterns of human systems of communities and enable researchers and practitioners to better anticipate and analyze ways communities bounce back in the aftermath of disruptive hazard events.

Keywords Resilience curve archetypes, Human mobility, Disasters

The characterization of resilience in human systems is of primal importance when evaluating their performance during and after disasters[1–6]. The key characteristics of system response to disturbance, such as the degree of return to the original state, return time, rate of return, and efficiency, are crucial to understanding resilience. Past research emphasizes that different characteristics can lead to varying conclusions about a system's resilience, highlighting the complexity of defining and measuring resilience in systems[7]. Studies conducted in recent years have focused on characterizing resilience curves[8–10], which graphically represent the trajectory of a community's functionality or performance from the onset of a disaster to the eventual recovery[11–15]. Functionality-focused resilience curves are a valuable approach for understanding and anticipating specific system responses to perturbations induced by disasters. However, they represent only one dimension of the multifaceted concept of community resilience. It is important to note that community resilience is a broader concept encompassing social, economic, infrastructural, and ecological dimensions beyond the scope of this study. Researchers have explored community resilience through various frameworks focusing on social capital, community competence, economic development, and information communication. Our work focuses specifically on human mobility

Urban Resilience.AI Lab, Zachry Department of Civil & Environmental Engineering, 3136 TAMU, College Station, TX 77843-3136, USA. ✉email: chawei0207@tamu.edu

patterns as one measurable aspect of human systems within communities, rather than claiming to characterize comprehensive community resilience. However, the use of resilience curves has remained a mere conceptual and visual tool with limited data-driven characterization and empirical grounding. Empirical characterizations of resilience curves provide essential insights regarding ways different systems of communities absorb perturbations and recover from disruptions[16–18]. Resilience curves have also been primarily used in characterizing the vulnerability and recovery of infrastructure systems of communities during hazard events. Previous studies discussed the importance of understanding the recovery dimension in resilience[19]. The use of a clustering algorithm for classifying recovery curves offers a quantitative approach to assessing system responses during disruptions, particularly in the context of water distribution systems[20].

Limited studies have examined the characteristics of resilience curves in human systems of communities. In recent years, a number of studies have examined fluctuations in human mobility patterns during hazard events as a way to capture both the loss of functionality and subsequent recovery of human systems in communities[21–27]. Examining resilience curves associated with human mobility enables the capture of fluctuations in human activities in response to disruptive events, such as floods, wildfires, storms, pandemics, or conflicts[28–38]. Human mobility represents an important measurable aspect of human systems in communities, providing a window into how people's movement patterns adapt to disruptive events. Under normal circumstances, human mobility would be at an equilibrium state, signifying routine movement patterns. When a disruptive event occurs, human mobility usually decreases as people seek shelter or infrastructure is disrupted, reflected by a dip in the resilience curve. Post-disaster, human mobility gradually recovers as people start to adapt, recover, and resume their routines[39]. The fluctuations in human mobility patterns can be captured to construct the resilience curve of human systems of communities. While the resilience curves in our study specifically focus on human mobility patterns, this approach is distinct from other uses of the term 'resilience curve' in the literature. Despite the growing number of studies examining resilience of human systems using human mobility patterns, limited attention has been paid to the resilience curve archetypes and their fundamental properties using empirical data. The specification of empirical resilience curve archetypes and their properties is essential to improve our understanding of the resilience patterns of human systems of communities and to enable researchers and practitioners to better anticipate and analyze ways communities bounce back in the aftermath of disruptive hazard events[40,41].

Recognizing this important knowledge gap, the primary objective of this study is to examine the presence of universal archetypes in human mobility resilience curves and delineate their fundamental properties. Specifically, we seek to address two specific research questions: (1) What are the primary archetypes of the human system resilience curves? and (2) What fundamental characteristics explain the behavior of different resilience curve archetypes? To assess the extent of functionality loss, we measure the degree of human mobility change by computing the number of trips going in and out of a given area. For our analysis, we utilize high-resolution location-based mobility data related to multiple extreme weather events in the United States. In total, we constructed more than 2000 empirical resilience curves representing different regions and hazard events. Accordingly, we examined and computed the main features of each resilience curve and subsequently classified them based on their main features into a set of universal archetypes. The following sections discuss the study data and methods.

Data description

This study collected and analyzed data from the following major hazard events in the United States: Hurricane Ida, Hurricane Harvey, Hurricane Laura, and Winter Storm Uri. Hurricane Ida, a Category 4 storm, struck in August 2021, causing its most profound devastation in Louisiana. Hurricane Ida later moved on to cause significant flooding and damage in the northeastern U.S., particularly impacting New York and New Jersey. Hurricane Harvey, also a Category 4 storm, made landfall near Rockport, Texas, in August 2017, then unleashed catastrophic flooding on the Houston metropolitan region. The impact was so severe that it ranks among the most damaging natural disasters in U.S. history. Category 4 storm Hurricane Laura in August 2020 majorly affected the Gulf Coast of the U.S., impacting parts of Louisiana and Texas and leaving a trail of destruction in its wake. In 2021, Winter Storm Uri swept across multiple states, with Texas being the most affected. Bringing low temperatures, snow, and ice, Uri led to extensive power outages, immense property damage, and several tragic fatalities. The storm's severity was such that Texas's power grid was overwhelmed, resulting in widespread blackouts across the state. These four events were chosen due to significant disruptions across the impacted regions. The data collection timeframes for each event were established according to the event's start date. Specifically, data collection commenced 9 days before the initiation of extreme weather events and spanned a total 35 days for such occurrences. In the case of the winter storm event, the data collection timeframe was limited to 24 days due to data availability constraints. The baseline periods—normal (steady-state) periods without perturbations from natural phenomena disasters—are set in the first week of the data collection timeframes. The mobility flow during this period is viewed as baseline performance.

Considering the variability in community sizes and to ensure a comparable assessment across diverse population densities, we implemented a minimum threshold of daily visits. Each census tract included in the study required a baseline of at least 50 daily visits before the event to be considered for analysis. This threshold was established to reduce the potential bias that could arise from smaller communities where each individual's movements might disproportionately affect the observed mobility rates. The 50-visit threshold serves as an inclusion criterion for census tracts in our analysis rather than a calculation parameter for baseline performance. While the actual range of daily visits varies considerably across census tracts (from our minimum threshold to several thousand visits in densely populated areas), this criterion ensures sufficient data volume to produce statistically meaningful resilience curves while respecting privacy requirements from our data provider. Each

included census tract's baseline is then individually calculated from its own pre-disaster daily trip volume, regardless of the absolute number of visits.

In establishing a baseline for daily trips during each event, we accounted for variations between weekdays and weekends to ensure a robust assessment of normal mobility patterns. Specifically, we calculated the baseline for weekday visits by averaging the number of trips from Monday to Friday and separately averaged the baseline for weekend visits for Saturday and Sunday. This approach allows us to compare mobility on individual weekdays to the average weekday baseline and similarly for the weekends. By using separate baselines for weekdays and weekends, we mitigate the effect of day-to-day variability within these categories, ensuring that our analysis more accurately reflects typical pre-event conditions. Deviations from these baselines are then utilized to assess the impact and recovery patterns during the event periods.

Table 1 summarizes the data collection details for each event. 402, 786, 402 and 786 empirical resilience curves are produced for affected areas during Hurricane Ida, Hurricane Harvey, Hurricane Laura and Winter Storm Uri. Adding up to a total of over 2000 resilience curves.

To construct the empirical resilience curves, we used a location-based dataset obtained from Spectus, a company that collects vast amounts of anonymous location information from approximately 70 million mobile devices in the United States through a privacy-compliant framework. This data is gathered when users voluntarily opt in to location services provided by partner apps. Spectus captures data from nearly 20% of the U.S. population, representing around one in four smartphone users. The location-based data from Spectus has proven valuable in previous research[4,31] to be representative in terms of capturing human mobility and travel mode detection due to its high spatiotemporal resolution. To safeguard user privacy, Spectus de-identifies the collected data and applies additional privacy measures, including obscuring home locations at the census-block group level and removing sensitive points of interest. The device-level data encompasses anonymized individual location information, ID, location coordinates, and timestamps. To ensure privacy preservation, Spectus offers access to its data, tools, and location-based datasets from other providers through a data cleanroom environment. The locations visited by each device are determined by identifying the census tract polygons each device resides in. The trajectory of a device's movement is then established based on the precedence relationship of their visit times. Daily trip counts between census tracts are aggregated at a census-tract level. For further analysis, a human mobility network is created using the daily trip counts among each census-tract pair. In this study, the focus lies on examining the fluctuation of total mobility flow in each census tract. Inflows and outflows are aggregated (summation), as their separation within the period of interest does not yield additional information for characterizing resilience curves. This is because inflow and outflow are proportional to the total flow and share the same flow pattern based on our preliminary investigation.

Methodology

Our analysis framework consists of the following components: (1) constructing the resilience curves; (2) extracting the key features of resilience curves; (3) finding the universal resilience curve archetypes and (4) specifying the main properties of the archetypes. Figure 1 depicts the overview of the analysis framework.

Our initial step focused on constructing empirical resilience curves associated with human mobility of census-tract populations across the four hazard events examined in the study. These empirical resilience curves are constructed by comparing the number of trips each day within the 35-day data-collection timeframe with the baseline (steady-state) number of trips for each census tract. The baseline number of trips serves as the baseline functionality of each census tract. For example, if the number of trips observed on a particular day during Hurricane Ida is 70% of the baseline value, then the remaining system functionality is 70%; the impact extent is 30%. Figure 2 shows a conceptual resilience curve, critical temporal points that signal transitions, and resilience features characterizing the curve. Each resilience curve is composed of critical temporal points: t_h (exposure to hazard): the time when the system first experiences the disruptive event; t_e (initial system disruption): the time when the system experiences the maximum disruptive effects; t_d (end of cascading failures): the time point when disruption starts to diminish; t_s (beginning of system recovery): the onset of the system's recovery period; t_f (completion of system recovery): the time point when the system is considered to have fully recovered and t_c (maximum recovery time): the complete end of the event, marking a return to normal conditions. t_f is determined by identifying the point at which the system's performance stabilizes at a new state, regardless of whether it matches the pre-event level. This approach aligns with the understanding that recovery may not necessarily mean a return to original conditions but could represent a new stable state. Stability is assessed by observing if the system's performance levels off and regularly fluctuate around a consistent level for a significant duration. To ensure consistent determination of t_f (completion of system recovery), we applied specific quantitative criteria in an automated procedure. A system is considered to have reached a new stable state when either: (1) performance returns to 100% of the pre-disaster baseline, or (2) performance reaches at least 85% of baseline and maintains stability (fluctuating within ±10% range) for at least five consecutive days. These thresholds were established

Event	Type	Affected areas	Number of census tracts	Event start date	Data collection time frame
Ida	Hurricane	Louisiana	402	2021/8/28	2021/8/19–2021/9/23
Harvey	Hurricane	Texas	786	2017/8/24	2017/8/15–2017/9/30
Laura	Hurricane	Louisiana	402	2020/8/27	2020/8/18–2020/9/22
Uri	Winter Storm	Texas	786	2021/2/13	2021/2/4–2021/2/28

Table 1. Summary of the weather events selected for this study.

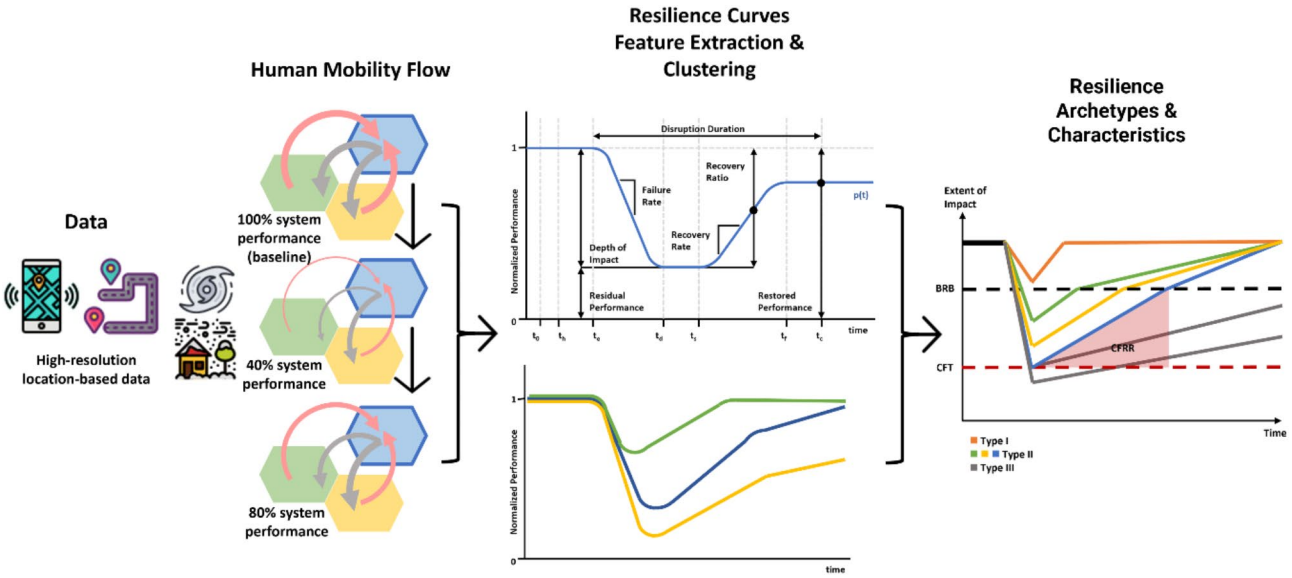

Fig. 1. Overview of analysis framework: Location-based data are analyzed to estimate mobility flow as a proxy for the functionality of human systems. Key resilience features, including the critical transition time points, are extracted from the human mobility resilience curves for each census tract. Based on their features, resilience curves were clustered to specify universal archetypes. The archetypes for human mobility resilience curves are examined to delineate their fundamental properties.

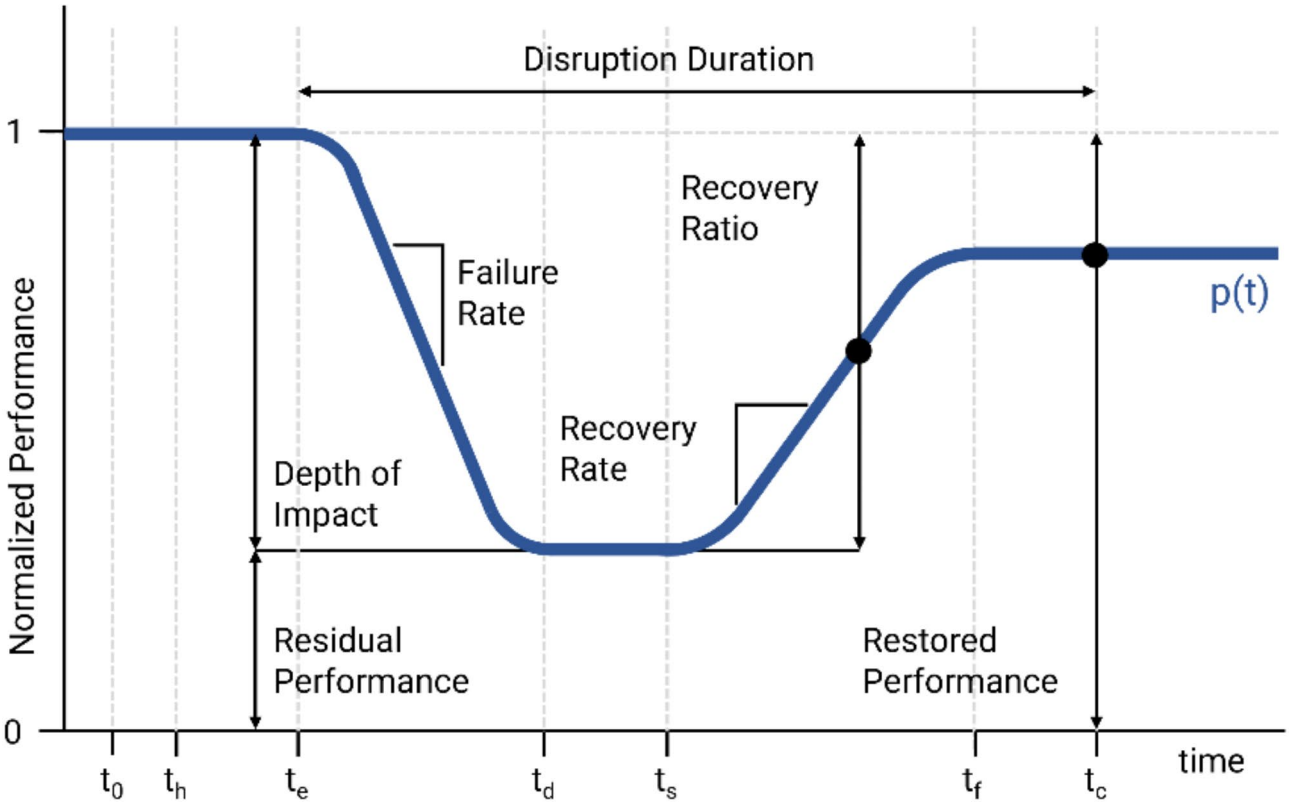

Fig. 2. Illustrative features for a conceptual resilience curve. Metrics may be derived with respect to performance p(t). In this illustration, the system does not fully recover within the control interval, so disruption duration may be undefined. The area above the resilience curve represents cumulative impact, while the area under the resilience curve represents cumulative performance.

based on empirical observations of typical pre-disaster fluctuation patterns and findings from our related studies examining post-disaster recovery trajectories. In cases where a system's performance does not meet these criteria within our observation timeframe, we consider recovery incomplete, which is valuable information in itself for characterizing the severity of impact and recovery challenges. These points encapsulate the timeline of the event and the corresponding system performance. Note that there is a single recovery rate in this conceptual resilience curve in Fig. 2. However, it is possible that we can observe bimodal recovery, which means we can find a turning point during the recovery process that the recovery rates before and after it are significantly different.

The subsequent step involves extracting key features from the resilience curves. The selection of key features is based on a review of the literature related to the characteristics of resilience curves (Table 2)[42,43]. The key features collected in the study can be grouped into multiple categories, including "magnitude", "duration", "integral", "rate" and "stability". Note that residual performance and depth of impact are not used simultaneously in this study because they are correlated and might cause problems in the implementation of the k-means algorithm. Thus, we only kept residual performance in the analysis. Similarly, we only used cumulative impact and left out cumulative performance. The temporal stability (d) is measured as inverse standard deviation of residual around the slope (b) of regression of relative function over time. The calculation is detailed in Table 2.

To mitigate noise and enhance the curves' discernibility, we employed a Savitzky-Golay filter after comparing the performance of multiple common smoothing techniques, such as rolling average and interpolators. However, curve smoothing should be applied judiciously to avoid potential over-smoothing, which could obscure important details. To reliably record the system resilience performance, we use the smoothed curve only for computing features related to integral and rate features and compute the other features from the original resilience curves. Upon completion of this step, the resilience curve for each census tract is represented by a vector of multiple key resilience features. It is important to note how we handle mobility values that exceed the baseline (> 100%). Such values are treated as natural system fluctuations and incorporated into our analysis without adjustment. In pre-disaster periods, these elevated values may represent evacuation activities or normal day-to-day variations. In post-disaster periods, they may represent a new equilibrium state or temporary activity surges during recovery. For calculation of metrics such as 'cumulative impact,' we specifically focus on the post-disaster period, measuring the area between the 100% performance line and the resilience curve.

Next, we perform clustering algorithms to classify resilience curves based on the key features to examine whether these clusters represent different universal archetypes. For testing different clustering algorithms, we used the elbow method and silhouette scores. Based on these metrics, we chose k-means clustering, which is a widely used technique due to its efficiency and simplicity. The k-means algorithm partitions the data into k distinct, non-overlapping subsets (or clusters), with each data point belonging to the cluster with the closest mean. After clustering, we proceed to compute an average resilience curve for each cluster. This step provides us with a representative curve that encapsulates the typical behavior for each cluster.

In the last step, we aim to find out the fundamental properties of the resilience curve archetypes. While our data resolution allows us to capture the daily fluctuation of recovery rates, we simplify these variations into piecewise linear segments by applying multivariate adaptive regression splines (MARS) on the representative curve of each cluster. MARS is a form of regression technique that automatically identifies the main turning points (knots) and slopes (system performance change rates) in the data. Although MARS is nonparametric in the sense that it doesn't assume a specific functional form for the relationship between variables, we controlled the model's complexity by setting specific control parameters, particularly the maximum number of basis functions (knots) allowed in the model. This approach enabled us to define the appropriate complexity of the piecewise linear model, ensuring that it adequately captures the predominant recovery dynamics while avoiding overfitting to minor daily fluctuations. The number of knots was carefully selected through cross-validation to balance model fit and interpretability, resulting in models that effectively represent the essential features of the resilience curves. Our analytical approach follows a systematic process to identify resilience patterns without arbitrary parameter selection. The clustering of resilience curves based on objectively calculated features allows natural

Types	Metrics	Formula	Definition
Magnitude	Residual performance	$p(t_d)$	System performance following the disruption, generally after cascading failures.
	Depth of impact	$1\text{-}p(t_d)$	Complement of residual performance.
	Restored performance	$(p(t_f) - p(t_d))/(p(t_e) - p(t_d))$	System' s performance after recovery efforts are complete.
Duration	Disruption duration	$t_f - t_e$	Entire period of degraded performance.
	Recovery duration	$t_f - t_d$	Period of the recovery phase, starting from the lowest performance.
Integral	Cumulative impact	$\int 1 - p(t)\, dt$	Integrated difference between performance and its reference.
	Cumulative performance	$\int p(t)\, dt$	Complement of cumulative impact.
Rate	Failure rate	$(p(t_d) - p(t_e))/(t_d - t_e)$	Resilience and adaptive capability at failure phases.
	Recovery rate	$(p(t_f) - p(t_s))/(t_f - t_s)$	Restorative capability at recovery phases.
Stability	Temporal stability	$d = 1/\text{std}(\text{residual}_b)$ $\ln(\text{recovery rate} / \text{average recovery rate}) = i + b * t$	Performance fluctuations around the trend. No benchmark, a larger d corresponds to lower fluctuations.

Table 2. Key resilience features extracted from the resilience curve regarding human mobility. Recovery for clustering.

groupings to emerge directly from the data. For each cluster, the representative aggregate curve reflects the collective recovery processes of all individual curves within that grouping. The MARS regression subsequently identifies critical transition points and recovery rates that characterize these dynamics, functioning as a pattern detection tool rather than imposing predetermined structures. This methodological approach enables us to distill complex, variable recovery behaviors into generalizable archetypes with clear, practical thresholds and transition points that characterize human mobility recovery following different levels of disruption. Common structures among these simplified representative curves can be observed. This approach allows us to balance data representativeness, model complexity and practical concerns. The common structures or characteristics will serve as our criteria for classifying archetypes. By identifying the archetypes, we can anticipate system performance effectively.

Results

We implemented the method described in the previous section on the data collected from Hurricane Ida, Hurricane Harvey, Hurricane Laura and Winter Storm Uri. Evaluation metrics for k-means clustering, such as the elbow method and silhouette score, suggest that the optimum number of clusters for the events is between 5 and 7 (see the Appendix). Among the clusters, one or two clusters can be viewed as outliers which we would remove for the interpretation of results. After the clustering and cleaning, we performed MARS to identify the critical turning points as the slope of line segments between these points. Figures 3, 4, 5 and 6 show the original average resilience curve (empirical data), the average resilience curve through smoothing and MARS (piecewise linear representation), critical turning points and slopes of the line segments between the turning points for each cluster. They demonstrate how MARS accurately reflects the underlying data, with attention paid to ensure that the structures captured are not artifacts of the modeling process but are reflective of the observed recovery dynamics. Each figure represents the resilience pattern of a specific event and the same colors in different figures do not indicate same types of clusters. We use clusters H1,2,3,… for Hurricane Harvey, clusters I1,2,3,… for Hurricane Ida, clusters L1,2,3,… for Hurricane Ida and clusters U1,2,3,… for Winter Storm Uri.

It is important to note that the system functional performance on the y-axis in Figs. 3, 4, 5 and 6 represent percentages relative to the pre-disaster baseline (100%). Values naturally fluctuate around this baseline during pre-disaster periods, with values above 100% representing normal day-to-day variations or potential evacuation activities. The resilience curves will not necessarily return to exactly 100% after a disaster, as systems may: (1) reach a new stable state at a different performance level, (2) gradually return to baseline beyond our observation period, or (3) achieve full recovery to baseline within the observation period. In Figs. 3, 4, 5 and 6, dotted lines

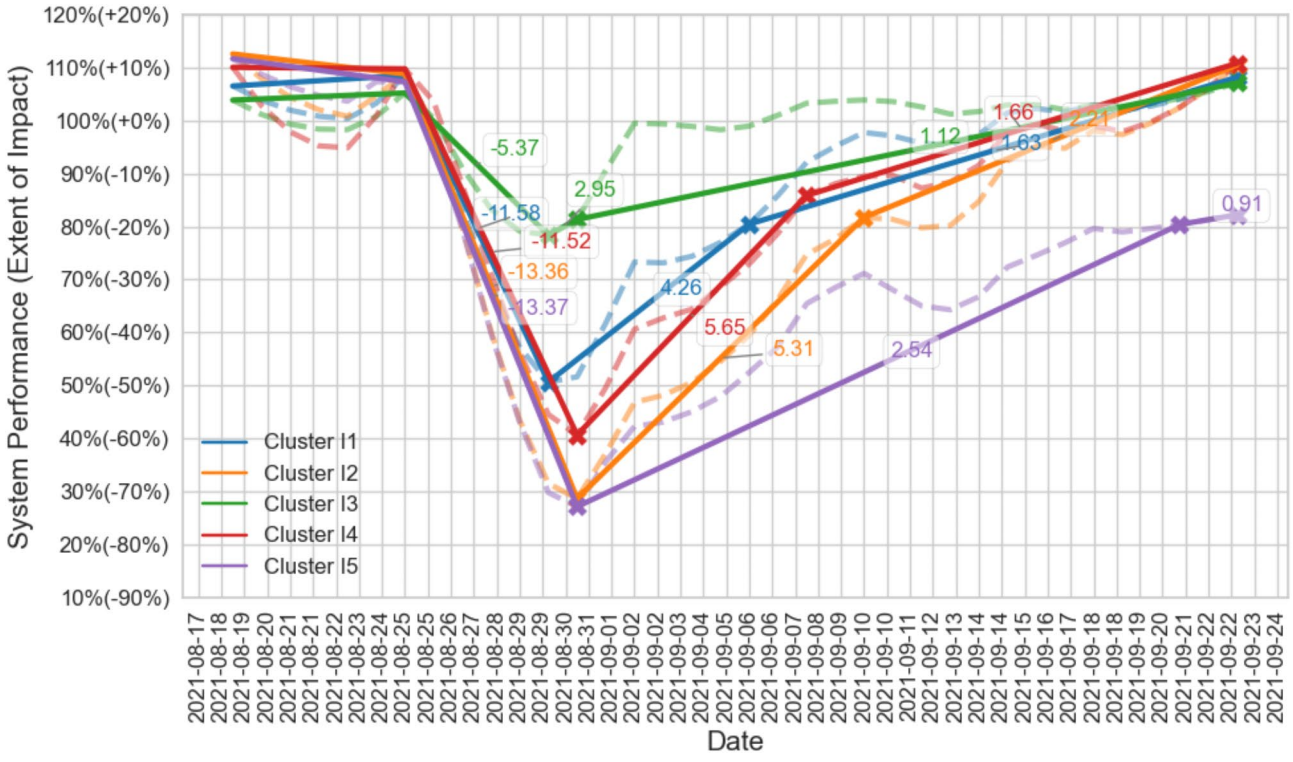

Fig. 3. Human mobility resilience curve clustering for Hurricane Ida. Each dashed curve represents the original average resilience curve of each cluster. Each solid curve represents the MARS regression on the average resilience curve of each cluster; the numbers represent failure rates and recovery rates. The extent of impact ranges from 20–70%. The turning point of bimodal recovery rate can be seen in clusters I1, I2 and I4 when the system recovers to between 80–90% of performance. Cluster I3 represents areas with relatively low impact and fast recovery. Cluster I5 represents areas with large impact and slow recovery.

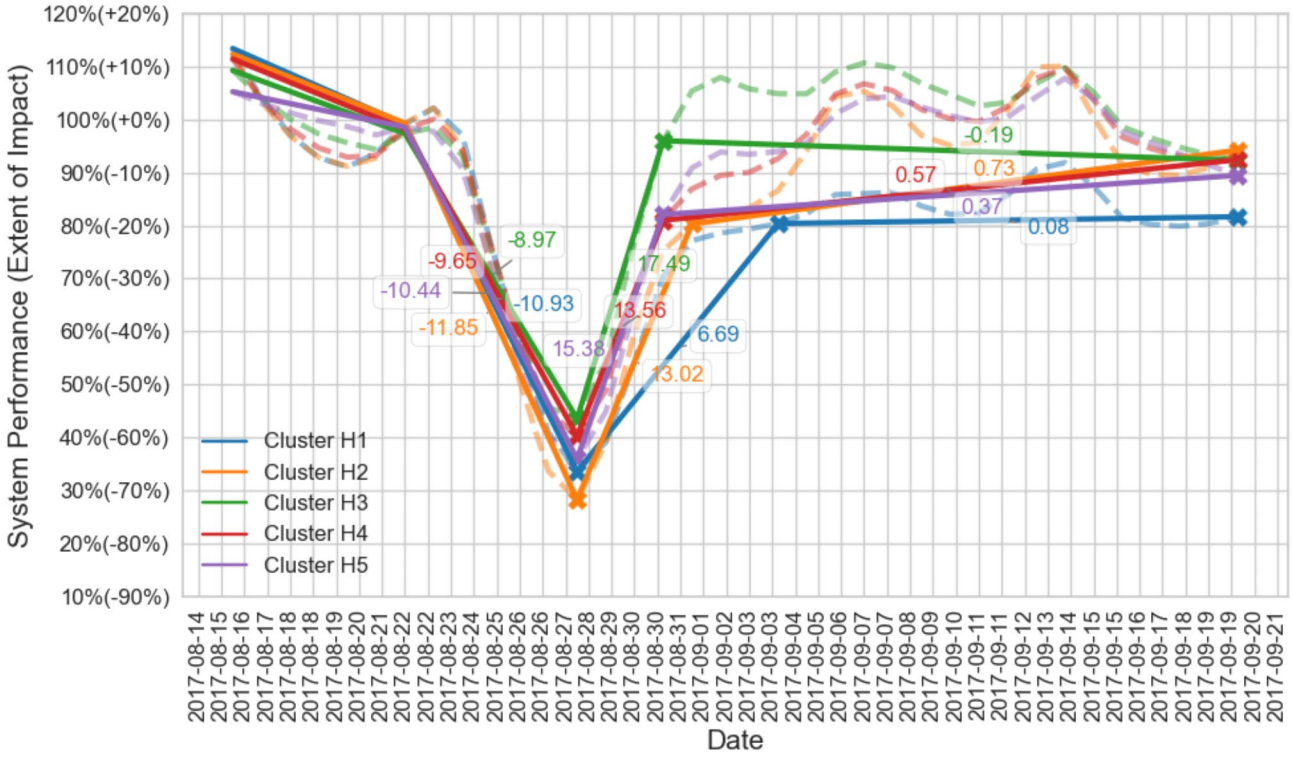

Fig. 4. Human mobility recovery clustering for Hurricane Harvey. Each dashed curve represents the original average resilience curve of each cluster. Each solid curve represents the MARS regression on the average resilience curve of each cluster; the numbers represent failure rates and recovery rates. The extent of impact ranges from 55–70%. The turning point of bimodal recovery rate can be seen in clusters H1, H2, H4, and H5 when the system recovers to between 80–90% of performance. Cluster H3 represents areas with relatively low impact and fast recovery.

represent the aggregated actual resilience curves for each cluster, while solid lines show the MARS regression results based on these empirical curves. These regression lines help identify critical transition points and recovery rates while filtering out minor fluctuations.

The shapes of resilience curves are all triangular instead of trapezoidal due to the more adaptive nature of human systems than infrastructure systems. Human mobility starts to recover immediately after the shock, while infrastructure systems may experience a sustained period of impact before their functionality starts recovering. The areas with larger impact are either the ones with communities with larger populations or coastal areas (specifically for hurricane events), which is intuitive.

Figure 3 shows the clustering results for Hurricane Ida in which the extent of impact varies, ranging from 20% to 70%. We can observe that except for cluster I5, all the other clusters fully recover at some point within our data collection timeframe. Cluster I3 reaches full recovery before other clusters, which exhibit a rapid upward trajectory after its relatively minor impact, contrasting with other clusters that show more gradual recovery patterns. Based on this result, if the impact extent exceeds 70%, then a region may take much longer to fully recover, which is not captured due to our data collection timeline. Except for cluster I3, we observe a significant slow-down in the recovery rate after passing a certain level of system performance in all the other clusters, 20% in this case.

Figure 4 shows the clustering results for Hurricane Harvey; the extent of impact ranges from 55 to 70%. We can observe evidence that the system performance of clusters H2, H3, H4, and H5 tends to oscillate regularly between a range of 90–100%, indicating full recovery within our data collection timeframe. The system performance level for cluster H1 after the disaster has reached 90% but does not have enough evidence to conclude a full recovery. For all the clusters, we see a significant decrease in the recovery rate after achieving a certain level of system functional performance, 80% in this case. This implies that after an initial recovery phase, the segments of the piecewise curves, though flatter, are still considered part of the recovery process as the system approaches a new stable state.

Figure 5 shows the clustering result for Hurricane Laura; the extent of impact ranges from 50 to 85%. We can observe evidence that the system performance of clusters L2 and L4 has reached 100%, indicating full recovery within our data collection timeframe. The system performance level for cluster L1 after the disaster has reached 80% and does not have enough evidence to conclude a full recovery. The system performance of Cluster L3 has reached almost 60%. Additionally, after reaching a specific threshold of system functionality, 80% in this instance, there is a noticeable decline in the recovery speed across the other clusters.

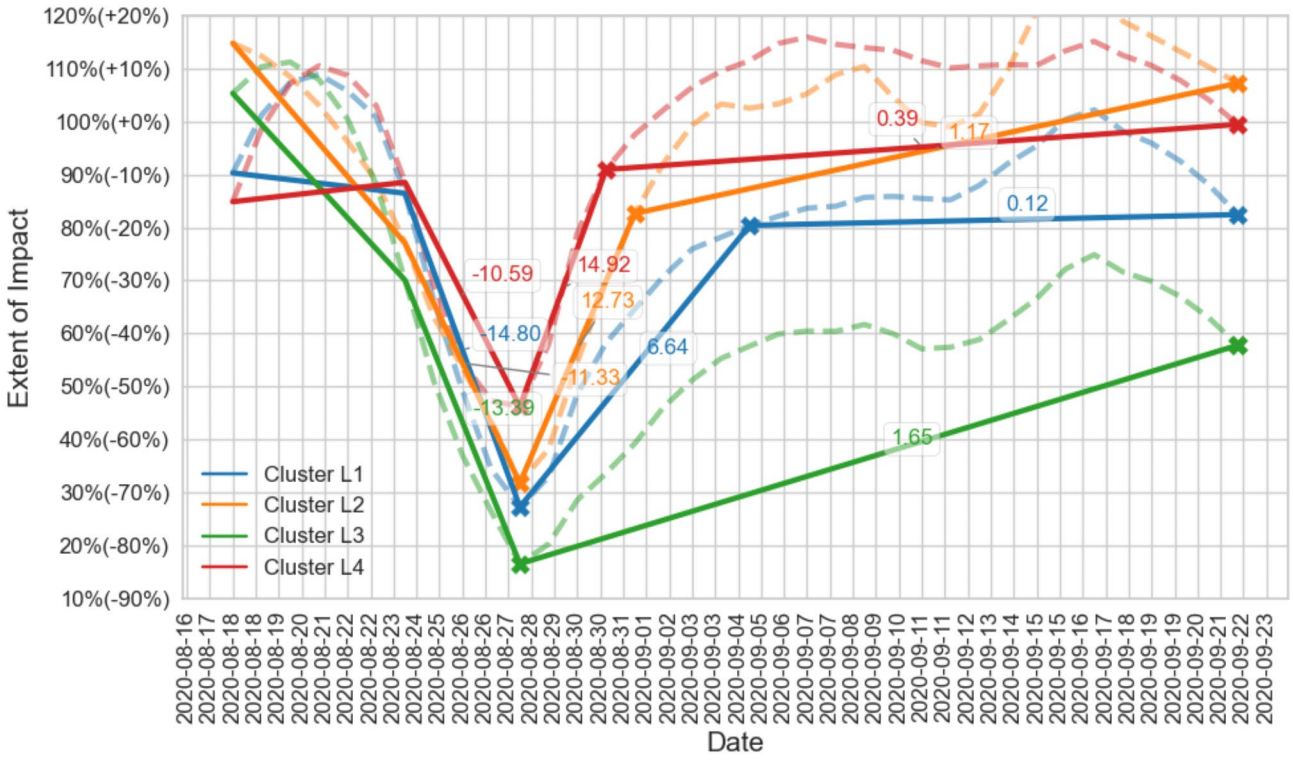

Fig. 5. Human mobility recovery clustering for Hurricane Laura. Each dashed curved represents the original average resilience curve of each cluster. Each solid curve represents the MARS regression on the average resilience curve of each cluster; the numbers represent failure rates and recovery rates. The extent of impact ranges from 50–85%. The turning point of bimodal recovery rate can be seen in clusters L1, L2, and L4, when the system recovers to between 80–90% of performance. Cluster L3 represents areas with large impact and slow recovery.

Figure 6. Human mobility recovery clustering for Winter Storm Uri. Each dashed curved represents the original average resilience curve of each cluster. Each solid curve represents the MARS regression on the average resilience curve of each cluster; the numbers represent failure rates and recovery rates. The extent of impact ranges from 40 to 60%. The turning point of bimodal recovery rate can be seen when the system recovers to between 80 and 90% of performance.

The results for the selected events revealed multiple important insights regarding fundamental properties of resilience curve archetypes of human mobility. Figure 7 shows the conceptual resilience curve resilience archetypes found in our empirical study. The three archetypes are as follows: Type I: This archetype comprises areas that experienced the least impact and exhibited relatively rapid recovery. Human mobility in these regions resumed quickly, showcasing efficient recovery processes. Type II: Areas with resilience curves of this archetype encountered moderate levels of impact. Notably, we observed a bimodal recovery rate, where the system's recovery speed significantly slowed down upon reaching a certain functional performance level. This bimodal phase transition was distinct from the initial recovery and had a noticeable impact on the overall recovery process. Type III: Representing the most affected areas, this group demonstrated considerably slower recovery rates than the other archetypes. It took significantly longer for these regions to return to full system performance. We acknowledge the potential for more complex recovery patterns, such as trimodal recoveries; however, our dataset did not reveal clear evidence of such patterns within the scope of this study.

Further investigation into these three archetypes led to identification of significant critical thresholds and distinguishing properties of the archetypes:

Bimodal recovery breakpoint (BRB)

The BRB is the point at which the recovery rate changes. The BRB was specified at the impact extent of 20%. If the impact extent is less than the BRB, human mobility recovers swiftly after hazard perturbations. If the impact extent is greater than the BRB, however, human mobility initially recovers to the BRB level with a faster recovery rate; after the BRB is achieved, the recovery rate slows down. While the observation that recovery time correlates with impact extent might seem intuitive, the identification of specific thresholds like the BRB where recovery behavior fundamentally changes provides quantitative precision to what would otherwise remain a qualitative understanding, enabling more accurate prediction and modeling of recovery trajectories.

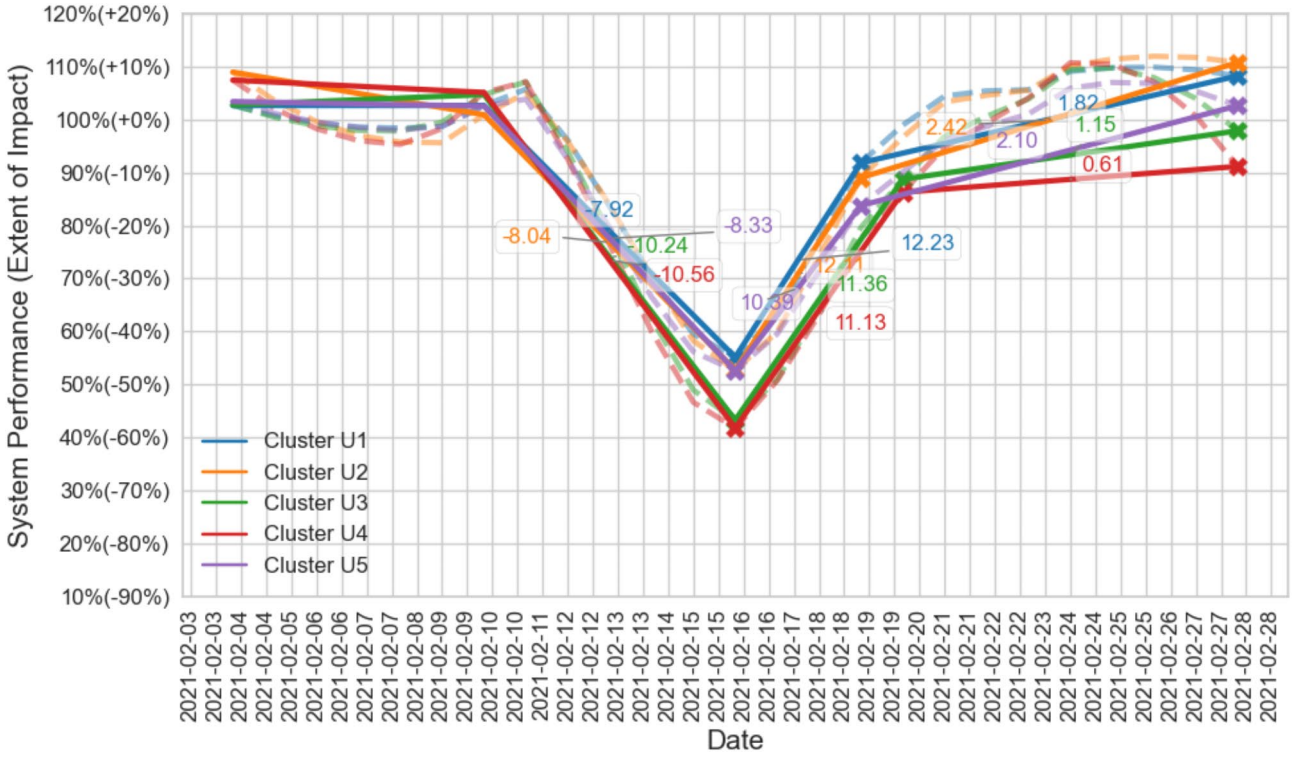

Fig. 6. Shows the clustering result for Winter Storm Uri; the extent of impact ranges from 40–60%. We notice that every cluster achieves full recovery within the duration of our data collection; however, once they reach a system functional performance threshold of 80%, there is a marked slowdown in their pace.

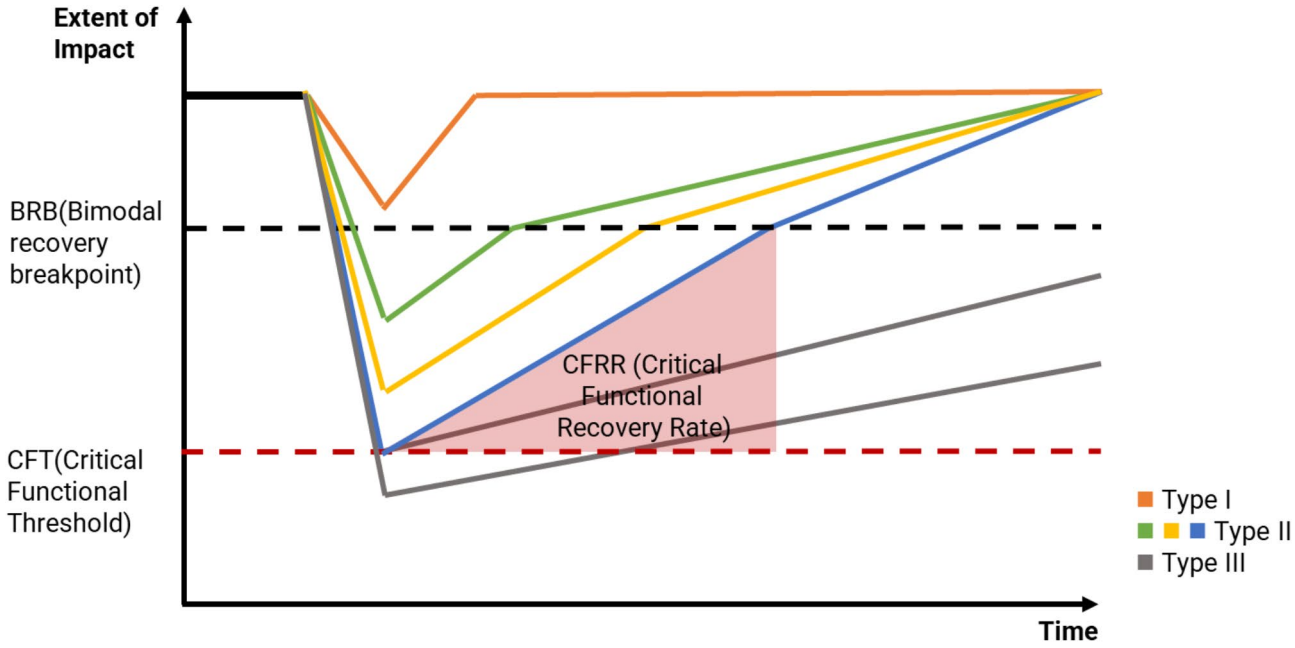

Fig. 7. Conceptual representation of the archetypes of human mobility recovery behavior post weather events. Each colored curve represents a cluster found in the analysis which is then further categorized into three archetypes. Critical functional threshold, bimodal recovery breakpoint, and critical functional recovery rate are the governing characteristics that separate the archetypes.

Archetypes	Extent of impact	Recovery rate	Description
Type I	I < BRB	$RR_1 > CFRR$	Least impact Fastest recovery Fully recovered
Type II	CFT > I > BRB	$RR_1 > CFRR$	Moderate impact Bimodal recovery rates Fully recovered
Type III	I > CFT	$RR_1 < CFRR$	Largest impact Slowest recovery

Table 3. The three archetypes of human mobility recovery behavior following weather events, and the governing characteristics that distinguish archetypes. I: Extent of impact, RR_1: Initial recovery rate right after impact, *BRB* Bimodal recovery breakpoint, *CFT* Critical functional threshold, *CFRR* Critical functional recovery rate.

Critical functional threshold (CFT)

The CFT is the impact extent beyond which the recovery of the system would proceed at a slow rate causing long recovery durations. The CFT for human mobility was identified with an impact extent of 60%. An impact extent greater than this threshold would lead to a significantly slower recovery speed. When the impact extent is close to CFT, two different behaviors (Type II - Blue and Type III) may be observed. The initial recovery rate (RR_1) is the determining factor in whether full recovery can be reached within a shorter period. When RR_1 is larger than the critical functional recovery rate (CFRR), which is 2.5% per day, we are likely to observe a Type II - Blue behavior. When RR_1 is less than CFRR, we are likely to observe a Type III behavior. Table 3 summarizes properties of different resilience curve archetypes related to human mobility and their fundamental properties. In summary, our examination of these distinct archetypes sheds light on resilience behavior of human mobility in hazard events. The identification of the BRB and CFT provides valuable insights into the recovery patterns of different areas, facilitating better anticipation and evaluations of ways different areas recover from hazard-induced perturbations.

All thresholds are defined relative to the pre-disaster baseline, enabling us to establish static reference points that allow for anticipation of future recovery states based on early post-disaster observations.

Regarding the recovery dynamics of Type II curves post-BRB, while the initial recovery rate is a critical indicator of resilience, the subsequent recovery phase is equally important. Our findings suggest that Type II curves generally exhibit a recovery pattern that leads to a complete recovery within a relatively short period, even if the recovery rate slows down after the BRB. This observation is based on historical data trends and recovery behaviors observed in past disaster events. However, the variability in recovery post-BRB highlighted in Figs. 4, 5, and 6 indicates that while these curves tend to recover, the exact trajectory can be influenced by various factors, including the nature and severity of the impact, community system resilience capabilities, and external aid. The historical recovery rate or the recovery rate observed in the aftermath of an actual disaster event can be utilized to anticipate the possible recovery trajectory.

Discussion and concluding remarks

The primary objective of this study is to explore the existence of universal archetypes in human mobility resilience curves when communities face weather hazards. Over the past two decades, resilience curves have been widely used to characterize the fluctuations in the functional performance of human and physical infrastructure systems of communities during disruptions; however, the majority of existing characterizations of resilience curves of communities do not consider variations in the types of resilience curve patterns a system might exhibit depending on the extent of impact. Also, most existing resilience curve characterizations focus on physical infrastructure; limited studies have empirically examined the characteristics of resilience curves in human systems of communities. It is important to emphasize that our analysis focuses specifically on human mobility resilience as one measurable aspect of community response to hazards, rather than claiming to characterize comprehensive community resilience, which encompasses broader social, economic, and infrastructure dimensions beyond the scope of this study.

Recognizing these important gaps, this study examined more than 2000 empirical resilience curves related to human mobility behaviors across multiple geographic regions and various weather events. The analyses examined datasets collected from Hurricanes Ida, Harvey, and Laura, and Winter Storm Uri in the United States. The results show that the resilience curves can generally be divided into three universal archetypes with low, medium, and high impact extent. The group with low impact exhibited the fastest recovery speed. In the second archetype with moderate impact extent, the recovery follows a bimodal rate: the initial recovery to the bimodal recovery breakpoint proceeds at a faster rate followed by a slower recovery rate after a breakpoint. This finding suggests that if the impact extent is not severe, human systems of community would strive to recover to the BRB as fast as possible. After the system functionality reaches BRB, the recovery rate slows. The existence of the bimodal recovery pattern might be a combination of two different behaviors. In the first stage of recovery, system functional performance quickly bounces back to around 80–90% of their normal functional performance because a large proportion of their daily activities return to normal. When this level of functional performance is achieved, the human system has a functional performance state; thus, the remaining recovery would follow a slower rate. In the third resilience archetype, when the impact exceeds critical functional threshold (i.e., 70%), the recovery rate would follow a slow rate with a consistent slope. This finding suggests that the critical

functionality threshold of 70% is the point beyond which the human system would struggle to recover. There are differences between the clusters of resilience curves observed from different types of events and different geographical areas; however, the three archetypes revealed in this study show good representativeness, covering all possible post-event human mobility recovery behaviors.

Recent studies in the field of complex systems have revealed that resilience, defined as a system's ability to maintain its basic functionality in the face of disturbances, is a characteristic shared by both human and physical systems. For instance, ecological networks, food webs, and even cyber-physical systems exhibit resilience patterns that mirror those observed in human systems. One study highlights the presence of universal patterns of resilience across different types of networks, including biological and technological systems[44]. This research emphasizes the ubiquity of resilience archetypes, like rapid recovery after mild disturbances and slower recovery following severe impacts, across a wide range of systems. Further exploration into the dynamics of physical systems presents a deeper understanding of how these patterns manifest in ecological and biological networks[45]. Their findings suggest that the resilience patterns observed in human systems, such as the ones identified in our study, have counterparts in the natural world, including population dynamics and mutualistic networks. These studies underscore the fundamental nature of resilience patterns, transcending the specific characteristics of human systems and extending to a broader array of complex systems.

While our study highlights the adaptive nature of human mobility in response to disasters, contrasting with the often slower and more predictable recovery trajectories of infrastructure systems, this does not necessarily imply that slower human return rates should directly translate into more proactive infrastructure restoration efforts. The correlation between human mobility and infrastructure recovery is complex and influenced by factors including the type of disaster, the resilience of the infrastructure itself, and the socio-economic dynamics of the affected community. For instance, in some cases, robust infrastructure might facilitate quicker human return, while in others, human mobility might recover independently of infrastructure due to adaptive behaviors and alternative solutions adopted by the community. Therefore, while enhancing infrastructure resilience is undoubtedly beneficial, the decision to escalate restoration efforts should be based on a comprehensive assessment of both infrastructure and human mobility data post-disaster. This nuanced understanding underscores the need for integrated recovery planning that considers the interdependencies between human behaviors and infrastructure systems.

Besides echoing the key findings from previous literature, findings of this study provide multiple important scientific and practical contributions. First, resilience curves have remained a mere conceptual and visual tool for understanding fluctuations in behaviors of community systems during and after hazard events. The absence of empirical grounding and specific characterization of resilience curves have hindered the ability to properly analyze and understand recovery trajectories of community systems. The findings of this study reveal the presence of universal resilience curve archetypes with specific properties (i.e., bimodal recovery breakpoint, critical functional threshold, and bimodal recovery rates) that enable evaluation of the way community systems behave in the aftermath of hazard-induced perturbations. Second, departing from the majority of the existing studies that focus on characterizing resilience in physical infrastructure, this study examined the resilience of human systems based on fluctuations in human mobility. By leveraging fine-grained location-based data from multiple hazard events, this study evaluated the functional performance of human systems of communities based on fluctuations in mobility flows to reveal universal resilience curve archetypes.

From a practical perspective, the outcomes of this study provide important insights for emergency managers and city officials. Based on the understanding of which areas are likely to belong to a certain archetype in an extreme weather event, we can anticipate the functional performance and recovery patterns. With the insights about the extent of impact and recovery trajectory for a short period after impact, decision-makers can take proactive actions to restore infrastructure and allocate resources to areas that are expected to follow a slow recovery rate. By assessing the extent of impact and recovery trajectory during the immediate post-event period, decision-makers can gain insights into an area's future performance. These contributions move us closer to a deeper understanding and a greater predictive insight regarding the resilience behaviors of community systems in hazard events. Future studies can build upon the findings of this study to examine empirical resilience curves and their characteristics in other community systems (such as infrastructure systems) to depart from using resilience curves as a mere conceptual and visual tool and reveal data-driven and empirical characteristics of resilience curves in different systems. For example, future studies can examine empirical data from other systems to evaluate whether similar universal resilience curve archetypes exist in other systems and if they exhibit properties such as critical functionality threshold and bimodal recovery rate. Such insights would move the field of community system resilience forward with empirical evidence needed to have a deeper and more predictive understanding of how different community systems behave during hazard-induced perturbations.

It is important to acknowledge the methodological challenges in determining precisely when a system reaches a steady state following disruption. While our study applied uniform criteria for this determination ($\geq 85\%$ performance with $\pm 10\%$ stability for 5 days), future research should explore more nuanced, context-specific approaches to defining recovery completion. Factors such as disaster type, pre-disaster system characteristics, and regional variations might necessitate adaptive thresholds. Additionally, longer observation periods would enable better characterization of long-term recovery trajectories, particularly for severely impacted systems that may require months or years to stabilize. These considerations highlight the importance of developing more sophisticated methods for monitoring and analyzing post-disaster system behavior across varied temporal scales. Recognizing the complexities in interpreting human mobility data during hurricane events, this study's findings serve as a preliminary step toward a more detailed understanding of community system resilience. It is clear that human mobility patterns are influenced by a multitude of factors, including the immediate response to the hurricane and the subsequent recovery phase. To elucidate the specific impact of hurricane intensity on community system resilience, we propose further research that extends beyond the immediate effects of the

hurricane. The correlation between human mobility recovery rates and the extent of physical damage from hazard events, along with the role of connectivity in affected locations, presents a valuable direction for future research. A detailed comparative analysis that examines the severity of such events against mobility pattern changes could yield insights into the influence of physical damage on community system resilience. Further exploration might also involve integrating connectivity metrics, like transportation network density and communication infrastructure robustness, to understand their impact on human mobility resilience. Multivariate analyses could be employed to unravel the complex interactions among these factors and their collective effect on the resilience of communities. High-resolution, location-based mobility data would be instrumental in advancing the empirical characterization of resilience curve archetypes and their defining properties, ultimately guiding predictive and responsive community recovery strategies.

While our findings reveal consistent resilience archetypes across different hazard types and geographical locations, we acknowledge that the generalizability of these archetypes requires further validation. Whether a specific area consistently exhibits the same archetype across different hazard events is particularly relevant for predictive applications. Our current evidence suggests that impact extent and initial recovery rate are stronger determinants of the resilience archetype than specific location characteristics or hazard types, which is promising for generalizability. The practical value of our approach lies in its potential for near-real-time assessment and prediction. By monitoring the early post-impact recovery trajectory and impact extent, decision-makers could classify an affected area into one of our identified archetypes and make informed resource allocation decisions based on the expected recovery pattern. For example, areas exhibiting characteristics of Type III resilience (severe impact with slow recovery rates) could be prioritized for additional support and intervention. Future research should focus on three key directions to enhance the predictive power and applicability of these archetypes: (1) expanding the empirical foundation by analyzing more diverse hazard types, intensities, and geographical contexts; (2) developing validation frameworks to test how consistently specific areas exhibit particular archetypes across multiple events; (3) creating predictive models that can classify areas into resilience archetypes based on early post-disaster signals and pre-existing community characteristics; and (4) model that can be applied on multiple disasters in effect simultaneously. Additionally, simulation studies could explore how various intervention strategies might alter the recovery trajectory of different archetypes, potentially enabling the transformation of a Type III recovery pattern into a more favorable Type II or even Type I pattern through targeted resource allocation.

This paper sheds light on the resilience of human mobility networks following disasters, offering insights that contrast with traditional infrastructure recovery models. However, the generalization of our results is subject to certain limitations, such as the scope of disaster events analyzed and the regional specificity of the data. Future research should aim to include a broader array of disaster types and geographies to enhance the robustness and applicability of our findings. Additionally, further studies could explore the causal relationships between infrastructure recovery and human mobility, potentially employing multi-layered network analyses to better understand and predict the dynamics at play. By addressing these limitations and expanding the scope of research, we can better inform disaster recovery strategies that are sensitive to both human and infrastructure resilience factors.

Data availability

All data were collected through a CCPA- and GDPR-compliant framework and utilized for research purposes. The data that support the findings of this study are available from Spectus (https://spectus.ai/product/), but rest rictions apply to the availability of these data, which were used under license for the current study. The data can be accessed upon request submitted to the providers (Spectus representative: Brennan Lake; email: blake@spectus.ai). The data was shared under a strict contract through Spectus' academic collaborative program, in which they provide access to de-identified and privacy-enhanced mobility data for academic research. All researchers processed and analyzed the data under a non-disclosure agreement and were obligated not to share data further or to attempt to re-identify data.

Code availability

The code that supports the findings of this study is available from the corresponding author upon request.

Received: 5 September 2023; Accepted: 25 March 2025
Published online: 07 April 2025

References

1. Alexander, D. E. Resilience and disaster risk reduction: an etymological journey, *Nat. Hazards Earth Syst. Sci.* **13**(11), 2707–2716. https://doi.org/10.5194/nhess-13-2707-2013 (2013).
2. Drabek, T. E. Human System Responses To Disaster: An Inventory of Sociological Findings. *Springer Science & Business Media.* https://doi.org/10.1007/978-1-4612-4960-3 (2012).
3. Gunderson, L. Ecological and Human Community Resilience in Response to Natural Disasters. *Ecol.Soc.* **15**(2). https://www.jstor.org/stable/26268155 (2010).
4. Hsu, C. W., Ho, M. A. & Mostafavi, A. Human mobility networks manifest dissimilar resilience characteristics at macroscopic, substructure, and microscopic scales. *Sci. Rep.* **13**(1), 17327. https://doi.org/10.1038/s41598-023-44444-5 (2023).
5. Roy, K. C., Cebrian, M. & Hasan, S. Quantifying human mobility resilience to extreme events using geo-located social media data. *EPJ Data Sci.* **8** (1), 18. https://doi.org/10.1140/epjds/s13688-019-0196-6 (2019).
6. Wang, Q. & Taylor, J. E. Patterns and limitations of urban human mobility resilience under the influence of multiple types of natural disaster. *PLoS One* **11**(1), e0147299. https://doi.org/10.1371/journal.pone.0147299 (2016).
7. Todman, L. C. et al. Defining and quantifying the resilience of responses to disturbance: a conceptual and modelling approach from soil science. *Sci. Rep.* **6**(1), 28426. https://doi.org/10.1038/srep28426 (2016).

8. Cimellaro, G. P., Reinhorn, A. M. & Bruneau, M. Framework for analytical quantification of disaster resilience. *Eng. Struct.* **32** (11), 3639–3649. https://doi.org/10.1016/j.engstruct.2010.08.008 (2010).
9. Gama Dessavre, D., Ramirez-Marquez, J. E. & Barker, K. Multidimensional approach to complex system resilience analysis. *Reliab. Eng. Syst. Saf.* **149**, 34–43. https://doi.org/10.1016/j.ress.2015.12.009 (2016).
10. Zobel, C. W. & Khansa, L. Characterizing multi-event disaster resilience. *Comput. Oper. Res.* **42**, 83–94. https://doi.org/10.1016/j.cor.2011.09.024 (2014).
11. Bruneau, M. et al. A Framework to Quantitatively Assess and Enhance the Seismic Resilience of Communities. *Earthquake Spectra* **19**(4), 733–752. https://doi.org/10.1193/1.1623497 (2003).
12. Hosseini, S., Barker, K. & Ramirez-Marquez, J. E. A review of definitions and measures of system resilience. *Reliab. Eng. Syst. Saf.* **145**, 47–61. https://doi.org/10.1016/j.ress.2015.08.006 (2016).
13. Manyena, S. B. The concept of resilience revisited. *Disasters* **30**(4), 434–450. https://doi.org/10.1111/j.0361-3666.2006.00331.x (2006).
14. Panteli, M., Mancarella, P., Trakas, D. N., Kyriakides, E. & Hatziargyriou, N. D. Metrics and Quantification of Operational and Infrastructure Resilience in Power Systems. *IEEE Trans. Power Syst.* **32**(6), 4732–4742. https://doi.org/10.1109/TPWRS.2017.2664141 (2017).
15. Tierney, K. & Bruneau, M. Conceptualizing and measuring resilience: A key to disaster loss reduction. *TR News*, (250). https://trid.trb.org/view/813539 (2007).
16. Bostick, T. P., Connelly, E. B., Lambert, J. H. & Linkov, I. Resilience science, policy and investment for civil infrastructure. *Reliab. Eng. Syst. Saf.* **175**, 19–23. https://doi.org/10.1016/j.ress.2018.02.025 (2018).
17. Ganguly, A. R., Bhatia, U. & Flynn, S. E. Critical Infrastructures Resilience: Policy and Engineering Principles. *Routledge*(2018).
18. Li, Y., Zhang, C., Jia, C., Li, X. & Zhu, Y. Joint optimization of workforce scheduling and routing for restoring a disrupted critical infrastructure. *Reliab. Eng. Syst. Saf.* **191**, 106551. https://doi.org/10.1016/j.ress.2019.106551 (2019).
19. Cassottana, B., Shen, L. & Tang, L. C. Modeling the recovery process: A key dimension of resilience. *Reliab. Eng. Syst. Saf.* **190**, 106528. https://doi.org/10.1016/j.ress.2019.106528 (2019).
20. Cassottana, B., Aydin, N. Y. & Tang, L. C. Quantitative assessment of system response during disruptions: an application to water distribution systems. *J. Water Resour. Plan. Manag.* **147** (3), 04021002. https://doi.org/10.1061/(ASCE)WR.1943-5452.0001334 (2021).
21. Chan, R. & Schofer, J. L. Measuring transportation system resilience: response of rail transit to weather disruptions. *Nat. Hazards Rev.* **17** (1), 05015004. https://doi.org/10.1061/(ASCE)NH.1527-6996.0000200 (2016).
22. Hong, B., Bonczak, B. J., Gupta, A. & Kontokosta, C. E. Measuring inequality in community resilience to natural disasters using large-scale mobility data. *Nat. Commun.* **12**(1), 1. https://doi.org/10.1038/s41467-021-22160-w (2021).
23. Kammouh, O., Zamani Noori, A., Cimellaro, G. P. & Mahin, S. A. Resilience assessment of urban communities. *ASCE-ASME J. Risk Uncertain. Eng. Syst. Part. A: Civil Eng.* **5** (1), 04019002. https://doi.org/10.1061/AJRUA6.0001004 (2019).
24. Martin-Breen, P. & Anderies, J. M. Resilience: A literature review. https://opendocs.ids.ac.uk/opendocs/handle/20.500.12413/3692 (2011).
25. Platt, S., Brown, D. & Hughes, M. Measuring resilience and recovery. *Int. J. Disaster Risk Reduct.* **19**, 447–460. https://doi.org/10.1016/j.ijdrr.2016.05.006 (2016).
26. Rus, K., Kilar, V. & Koren, D. Resilience assessment of complex urban systems to natural disasters: A new literature review. *Int. J. Disaster Risk Reduct.* **31**, 311–330. https://doi.org/10.1016/j.ijdrr.2018.05.015 (2018).
27. Zhang, W. & Wang, N. Resilience-based risk mitigation for road networks, *Struct. Saf.* **62**, 57–65. https://doi.org/10.1016/j.strusafe.2016.06.003 (2016).
28. Coleman, N., Gao, X., DeLeon, J. & Mostafavi, A. Human activity and mobility data reveal disparities in exposure risk reduction indicators among socially vulnerable populations during COVID-19 for five U.S. metropolitan cities. *Sci. Rep.* **12**(1), 1. https://doi.org/10.1038/s41598-022-18857-7 (2022).
29. Farahmand, H., Wang, W., Mostafavi, A. & Maron, M. Anomalous human activity fluctuations from digital trace data signal flood inundation status. *Environ. Plan. B Urban Anal. City Sci.* **49**(7), 1893–1911. https://doi.org/10.1177/23998083211069990 (2022).
30. Gao, X. et al. Early indicators of human activity during COVID-19 period using digital trace data of population activities. *Front. Built Environ.* **6**. https://doi.org/10.3389/fbuil.2020.607961 (2021).
31. Hsu, C. W., Liu, C., Nguyen, K. M., Chien, Y. H. & Mostafavi, A. Do Human Mobility Network Analyses Produced from Different Location-based Data Sources Yield Similar Results across Scales? *Comput. Environ. Urban Syst.* **107**, 102052. https://doi.org/10.1016/j.compenvurbsys.2023.102052 (2024).
32. Lee, C. C., Chou, C. & Mostafavi, A. Specifying Evacuation Return and Home-switch Stability During Short-term Disaster Recovery Using Location-based Data. *Sci. Rep.* **12**(1), 115987. https://doi.org/10.48550/arXiv.2201.05253 (2022).
33. Li, B., Fan, C., Chien, Y. H., Xsu, C. W. & Mostafavi, A. Mobility Behaviors Shift Disparity in Flood Exposure in U.S. Population Groups. *Int. J. Disaster Risk Reduct.* **108**, 104545. https://doi.org/10.1016/j.ijdrr.2024.104545 (2023).
34. Li, Q. et al. Disparate patterns of movements and visits to points of interest located in urban hotspots across US metropolitan cities during COVID-19. *R. Soc. Open. Sci.* **8** (1), 201209. https://doi.org/10.1098/rsos.201209 (2021).
35. Liu, Z., Liu, C. & Mostafavi, A. Beyond Residence: A Mobility-based Approach for Improved Evaluation of Human Exposure to Environmental Hazards. *Environ. Sci. Tech.* **57**(41), 15511–15522. https://doi.org/10.1021/acs.est.3c04691 (2023).
36. Rajput, A. A., Li, Q., Gao, X. & Mostafavi, A. Revealing Critical Characteristics of Mobility Patterns in New York City During the Onset of COVID-19 Pandemic, *Frontiers in Built Environment* **7**. https://doi.org/10.3389/fbuil.2021.654409 (2022).
37. Rajput, A. A. & Mostafavi, A. Latent sub-structural resilience mechanisms in temporal human mobility networks during urban flooding, *Sci. Rep.* **13**(1), 1. https://doi.org/10.1038/s41598-023-37965-6 (2023).
38. Tang, J. et al. Resilience patterns of human mobility in response to extreme urban floods, *Natl. Sci. Rev.* **10**(8), nwad097. https://doi.org/10.1093/nsr/nwad097 (2023).
39. Nicholson, C. D., Barker, K. & Ramirez-Marquez, J. E. Flow-based vulnerability measures for network component importance: experimentation with preparedness planning. *Reliab. Eng. Syst. Saf.* **145**, 62–73. https://doi.org/10.1016/j.ress.2015.08.014 (2016).
40. Chang, S. E. & Shinozuka, M. Measuring improvements in the disaster resilience of communities. *Earthq. Spectra*. **20** (3), 739–755. https://doi.org/10.1193/1.1775796 (2004).
41. Gao, H., Chen, Y., Mei, S., Huang, S. & Xu, Y. Resilience-Oriented Pre-Hurricane Resource Allocation in Distribution Systems Considering Electric Buses, *Proc. IEEE* **105**(7), 1214–1233. https://doi.org/10.1109/JPROC.2017.2666548 (2017).
42. Hillebrand, H. et al. Decomposing multiple dimensions of stability in global change experiments. *Ecol. Lett.* **21** (1), 21–30. https://doi.org/10.1111/ele.12867 (2018).
43. Poulin, C. & Kane, M. B. Infrastructure resilience curves: performance measures and summary metrics. *Reliab. Eng. Syst. Saf.* **216**, 107926. https://doi.org/10.1016/j.ress.2021.107926 (2021).
44. Gao, J., Barzel, B. & Barabási, A. L. Universal resilience patterns in complex networks. *Nature* **530**(7590), 7590. https://doi.org/10.1038/nature16948 (2016).
45. Tu, C., Grilli, J., Schuessler, F. & Suweis, S. Collapse of resilience patterns in generalized Lotka-Volterra dynamics and beyond. *Phys. Rev. E.* **95** (6), 062307. https://doi.org/10.1103/PhysRevE.95.062307 (2017).

Acknowledgements
This material is based in part upon work supported by the National Science Foundation under CRISP 2.0 Type 2 No. 1832662 and CAREER 1846069. The authors also would like to acknowledge the data support from Spectus. Any opinions, findings, conclusions, or recommendations expressed in this material are those of the authors and do not necessarily reflect the views of the National Science Foundation or Spectus.

Author contributions
All authors critically revised the manuscript, gave final approval for publication, and agree to be held accountable for the work performed therein. C.H. was the lead Ph.D. student researcher and first author, who was responsible for supervising data collection, performing final analysis, writing the majority of the manuscript and creating all the figures. A.M. was the faculty advisor for the project and provided critical feedback on the project development and manuscript.

Declarations

Competing interests
The authors declare no competing interests.

Additional information
Supplementary Information The online version contains supplementary material available at https://doi.org/10.1038/s41598-025-95909-8.

Correspondence and requests for materials should be addressed to C.-W.H.

Reprints and permissions information is available at www.nature.com/reprints.

Publisher's note Springer Nature remains neutral with regard to jurisdictional claims in published maps and institutional affiliations.